

Sustainable Food Technology

Accepted Manuscript

This article can be cited before page numbers have been issued, to do this please use: A. Celebioglu, K. Ertan, M. Aboelkheir and T. Uyar, *Sustainable Food Technol.*, 2026, DOI: 10.1039/D6FB00056H.



This is an Accepted Manuscript, which has been through the Royal Society of Chemistry peer review process and has been accepted for publication.

Accepted Manuscripts are published online shortly after acceptance, before technical editing, formatting and proof reading. Using this free service, authors can make their results available to the community, in citable form, before we publish the edited article. We will replace this Accepted Manuscript with the edited and formatted Advance Article as soon as it is available.

You can find more information about Accepted Manuscripts in the [Information for Authors](#).

Please note that technical editing may introduce minor changes to the text and/or graphics, which may alter content. The journal's standard [Terms & Conditions](#) and the [Ethical guidelines](#) still apply. In no event shall the Royal Society of Chemistry be held responsible for any errors or omissions in this Accepted Manuscript or any consequences arising from the use of any information it contains.

Sustainability spotlight

Orally fast-disintegrating nanofibrous web developed from natural cyclodextrin molecules presents a biocompatible platform for the delivery of caffeic acid. The inclusion complexes of cyclodextrin and caffeic acid are synthesized in aqueous medium in the absence of an additional toxic solvent, and nanofibers are generated from these complexes without using a carrier polymeric matrix via electrospinning technique. By adapting inclusion complexation, enhanced water solubility, fast-release, and improved antioxidant performance are provided for nutraceutical caffeic acid while eliminating the use of aggressive chemicals, which is quite common in conventional production techniques, having environmental and health loadings. This work endorses the global transition to a sustainable approach for the development of biocompatible materials having potential for use in food, biomedical, and cosmetic applications by contributing to eradicating the need for fossil fuel-based products.



ARTICLE

Cyclodextrin/Caffeic Acid Nanofibers with Enhanced Antioxidant Activity, Fast-Release and Fast-Disintegrating Properties

Asli Celebioglu^a, Kubra Ertan^{a,b}, Mahmoud Aboelkheir^a, Tamer Uyar^{a*}Received 00th January 20xx,
Accepted 00th January 20xx

DOI: 10.1039/x0xx00000x

Cyclodextrin (CD)/caffeic acid inclusion complex nanofibers having fast-release and orally fast-disintegrating features were generated using the electrospinning technique. Here, two types of hydroxypropylated CD (HP β CD and HP γ CD) were used to create electrospun nanofibers with two different molar ratios (1:1 and 2:1 CD:caffeic acid). Caffeic acid-incorporated pullulan nanofibers were also electrospun as a control sample. All nanofibrous webs exhibited homogenous morphology with free-standing and foldable features. Caffeic acid is a phenolic bioactive compound with poor solubility. A phase solubility study confirmed a significant increase in the solubility of caffeic acid by ~ 16 , 18-fold due to complex formation. Nanofibrous webs were successfully obtained with the initial caffeic acid contents (~ 5 -9% (w/w)) by protecting its chemical structure. The amorphized caffeic acid, combined with the unique features of nanofibers, enabled the achievement of faster disintegration, higher release rates, and better antioxidant activity for CD/caffeic acid nanofibers compared to the polymeric sample.

1 Introduction

Phenolic acids are biologically active compounds and a vital component of the human diet that possess commercial value in the cosmetic, food, health, and biomedical industries for their antioxidant, anti-aging, antitumor, antidiabetic, anti-inflammatory, and antibacterial properties.¹⁻³ They are primarily categorized into two subgroups: hydroxybenzoic and hydroxycinnamic acid. Hydroxycinnamic acids were reported to demonstrate stronger antioxidant activity compared to hydroxybenzoic ones due to the existence of an extra carbon-carbon double bond adjacent to the benzene ring, hence enhancing the conjugated π orbital system.¹ Caffeic acid, ferulic acid and *p*-coumaric acid are the most commonly known examples of hydroxycinnamic acids.³ Caffeic and ferulic acids, in both free and esterified forms, are the predominant phenolic acids found in most fruits and cereal grains, respectively, and the antioxidant activity of caffeic acid was found to be superior to other hydroxycinnamic acids due to its radical stability.^{1,4} Caffeic acid (3,4-dihydroxycinnamic acid) is synthesized via the secondary metabolism of numerous food products such as coffee beans, fruits, potatoes, olives, carrots, propolis, and also found in tea and wine.⁵ Besides antioxidant characteristic, caffeic acid exhibits neuroprotective⁶ and anti-inflammatory⁵ properties. Moreover, caffeic acid and derivatives has been reported to inhibit cancer by disrupting the migration and metastasis of cancer cells and promote the sensitivity of cancer cells against radiation and chemotherapy.⁷ Whereas caffeic acid

stands out for its superior bioactivity, its poor solubility and low thermal stability limit the application of this bioactive compound. Various encapsulation systems can be utilized to address these challenges, including emulsions⁸, liposomes⁹, nanoparticles¹⁰, fibers¹¹, and cyclodextrins.^{12,13} Moreover, there are several research reporting the encapsulation of caffeic acid into the nanofibers of carob flour/whey protein/polyethylene oxide¹⁴, poly (3-hydroxybutyrate)¹⁵, and poly(ϵ -caprolactone)/chitosan¹⁶ by electrospinning. Electrospinning, a simple and cost-effective method, offers various advantages in terms of nanofiber characteristics, including a high surface-to-volume ratio, adjustable diameter, mechanical flexibility, and a highly porous nanoweb structure¹⁷, during the encapsulation of bioactive compounds that have potential to be used in biomedical¹⁸ and food applications.^{19,20}

On the other hand, the distinctive structural feature of cyclodextrins (CDs), cyclic oligosaccharides, is an inner hydrophobic cavity that can form non-covalent host-guest inclusion complexes (ICs) with various bioactive agents, thereby increasing their solubility and stability.^{21,22} A study on the ICs of caffeic acid with different native CD types (α -CD, β -CD, and γ -CD) revealed that the antioxidant activity of caffeic acid was improved by inclusion complexation due to its greater solubility within the system.¹³ In another study, inclusion complexation of caffeic acid with α -CD resulted in better dissolution rates, which supports improving the bioavailability of caffeic acid.²³ In addition to being food-grade, certain types of CDs are certified as "generally recognized as safe" (GRAS) and included in the European food additives list and so CDs have also significant potential for industrial application in both food and pharmaceutical industries.²¹ Furthermore, the highly concentrated formulations of modified CDs including hydroxypropyl-alpha-cyclodextrin (HP α CD), methyl-beta-cyclodextrin (M β CD), hydroxypropyl-beta-cyclodextrin

^a Fiber Science Program, Department of Human Centered Design, College of Human Ecology, Cornell University, Ithaca, NY 14853, USA

^b Department of Food Engineering, Faculty of Engineering and Architecture, Burdur Mehmet Akif Ersoy University, Istiklal Campus, 15030 Burdur, Turkey

* Corresponding Author



(HP β CD), hydroxypropyl- γ -cyclodextrin (HP γ CD) in water or organic solvents enable the successful electrospinning of these systems into fast-disintegrating nanofibers without using any polymer.²⁴ The production of free-standing nanofiber from the ICs of modified CD and various types of polyphenol, including curcumin²⁵, catechin²⁶, resveratrol²⁷, and ferulic acid²⁸ has been also reported to attain the encapsulation of these bioactive compounds. Moreover, increased stability, solubility, and enhanced antioxidant activity have been achieved for the mentioned polyphenols through inclusion complexation with natural and non-toxic CD molecules. Here, water is the only solvent to form ICs and to perform solution-based electrospinning. In other words, there is no need to use an aggressive or toxic solvent system to dissolve the components and run the process, which is common in other production techniques or in the use of polymeric systems. Therefore, the electrospinning of CD IC nanofibers can be considered as a sustainable approach in order to develop biocompatible materials.

CD IC nanofibers can exhibit fast-disintegrating property, enabling their rapid dissolution or disintegration in the oral cavity without the need for water, similar to orally disintegrating tablets (ODTs).^{29,30} As in pharmaceutical applications, this approach may also offer a convenient route for the administration of nutraceutical compounds, not only for individuals with swallowing difficulties but also for the general population, while potentially enhancing bioavailability.³¹ In one of the related studies by Narayanan et al., the ICs of caffeic acid with β -CD and γ -CD were incorporated into electrospun nanofibers of poly(vinyl alcohol) (PVA) to produce antibacterial materials for food packaging applications.³² However, there are currently no reports in the literature addressing the development of a nanofibrous web from the ICs of caffeic acid and CD without the use of a carrier polymeric matrix, and which have high potential to be used as an orally fast-disintegrating delivery system. In this study, highly water-soluble modified CDs; HP β CD and HP γ CD were chosen to form ICs with caffeic acid at two different molar ratio (1:1 and 2:1 CD:caffeic acid) and to generate the free-standing nanofibrous webs (Fig. 1). Pullulan/caffeic acid nanofibers were also fabricated as a control sample. Pullulan is a water-soluble polysaccharide (~500 mg/mL) with a linear polymer chain structure composed of maltotriose units (three α -(1,4)-linked glucose units) connected via α -(1,6)-glycosidic bonds.³³ Due to its structural similarity to CDs (i.e., glucose subunits linked by α -1,4-glycosidic bonds) and its water solubility, pullulan was selected as a control carrier system to evaluate the potential differences arising from the use of a CD or a polymer.

The morphological, structural and thermal properties of the free-standing nanofibers of HP β CD/Caffeic acid (1/1), HP γ CD/Caffeic acid (1/1), HP β CD/Caffeic acid (2/1), HP γ CD/Caffeic acid (2/1) and pullulan/caffeic acid were assessed by several characterization techniques including SEM, ¹H-NMR, 2D-NMR, XRD, FTIR and TGA. The release kinetic models and the disintegration profiles were derived for all samples based on the results of the release and disintegration

tests. Additionally, antioxidant activity of the nanofibrous webs was determined by DPPH• radical scavenging method.

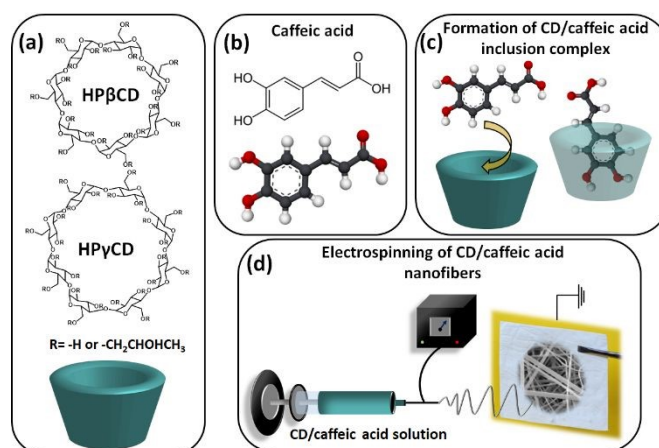


Fig. 1. The chemical structure of (a) HP β CD and HP γ CD, and (b) caffeic acid. (c) The schematic representation of CD/caffeic acid inclusion complex formation, (d) and the electrospinning of CD/caffeic acid nanofibers.

2 Materials and methods

2.1 Materials

Hydroxypropyl- β -cyclodextrin (HP β CD) (Cavasol W7 HP, DS: ~ 0.9) and hydroxypropyl- γ -cyclodextrin (HP γ CD) (Cavasol W8 HP Pharma, DS: ~ 0.6) were supplied from Wacker Chemie AG (USA) as a gift. Caffeic acid (C₉H₈O₄, >98%), as received pullulan (Mw: 300 000 g/mol, TCI America), methanol (\geq 99.8% (GC), Sigma Aldrich), dimethyl sulfoxide (DMSO, > 99.9%, Sigma Aldrich), 2,2-diphenyl-1-picrylhydrazyl (DPPH, \geq 97%, TCI America), and deuterated dimethylsulfoxide (*d*6-DMSO, 99.8%, Cambridge Isotope) were purchased. The experiments were conducted using MiliQ water, which has a resistance of 18.2 M Ω cm.

2.2 2D-NMR Measurement

Nuclear magnetic resonance (NMR) spectra of HP β CD/caffeic acid and HP γ CD/caffeic acid inclusion complexes (ICs) were recorded in D₂O using a 600 MHz Varian INOVA spectrometer operating at 599.50 MHz for proton detection. A 5 mm Varian HPX inverse broadband triple-resonance probe equipped with a single-axis pulsed field gradient was employed, and all measurements were performed at 25 °C. Standard pulse sequences provided by VnmrJ 3.2A software (Agilent Inc.) were used for data acquisition, while spectral processing and analysis were carried out with MestReNova 14.3.2-32681 (Mestrelab Research S.L.). For 2D ROESY experiments, the ROESYAD pulse sequence was applied with a mixing time of 200 ms. The acquisition parameters included 400 complex t_1 increments, 4 scans per increment, 32 dummy scans, a relaxation delay of 1.5 s, and an acquisition time of 0.3 s.



2.3 Phase solubility study

Here, excess amount of caffeic acid was mixed with the increasing concentration of CD (0 to 120 mM) in 5 mL of water. The aqueous systems were shaken on an incubator shaker (shielded from light at room temperature) for 24 h using 450 rpm. Afterwards, each suspension was filtered using PTFE filter (0.45 μm), and filtered systems were characterized by UV-vis-spectroscopy (PerkinElmer, Lambda 35, USA). The calibration curve ($R^2 \geq 0.99$) enabled the conversion of absorbance intensity values into the concentration (mM). The triplicate measurements were performed for each system and the phase solubility diagrams were plotted using the mean values \pm standard deviations. The binding constant (K_s) values were also determined using the equation given below;

$$K_s = \text{slope}/S_0(1-\text{slope}) \text{ (Eq. 1)}$$

where S_0 : intrinsic solubility of caffeic acid (~ 2.4 mM).

2.4 Electrospinning

The aqueous solutions of CD and pullulan were prepared using the solid concentration of 200 % (w/v) and 20 % (w/v), respectively. For the preparation of IC systems, two distinct molar ratios of modified CD to caffeic acid (1:1 and 2:1) were determined and caffeic acid powder was added to CD solutions accordingly. Pullulan/caffeic acid solution was prepared with ~ 5 % (w/w, in proportion to total sample amount) of caffeic acid concentration that corresponds to the active compound content of CD/caffeic acid samples generated with 2:1 (CD:caffeic acid) molar ratio. All aqueous systems were stirred overnight to promote the formation of the IC between CD and caffeic acid molecules. The viscosity measurements of the electrospinning solutions were conducted using a rheometer (AR 2000 rheometer, TA Instrument, USA) fitted with a 4° cone/plate (20 mm) spindle at a shear rate of 0.01–1000 s^{-1} at room temperature. The conductivity values of the same solutions were determined by conductivity meter (FiveEasy, Mettler Toledo, USA) at room temperature. The electrospinning solutions of CD, pullulan, CD/caffeic acid and pullulan/caffeic acid were introduced to the system via an individual 1 mL syringe fixed with a 23 G metallic needle. The syringe was horizontally inserted into the electrospinning equipment (Spingenix, model: SG100, Palo Alto, USA). A grounded metal collector was coated with a piece of aluminum foil and then positioned ~ 15 cm distant from the needle tip. The electrospinning process was conducted using a constant flow rate (0.5 mL/h) and a high voltage (10–15 kV) under the ambient conditions (~ 45 % relative humidity and 22°C).

2.5 Structural characterizations

The morphological examination of electrospun CD, pullulan, CD/caffeic acid and pullulan/caffeic acid nanofibers was carried out by scanning electron microscope (SEM, Tescan MIRA3, Czech Republic). The samples were coated with Au/Pd coating in order to prevent charging problems during analysis. SEM images of samples were captured at an accelerating voltage of 12 kV at a distance of 10 mm. Subsequently, ImageJ software

was used to compute the average diameter of electrospun fibers based on 100 randomly chosen nanofibers. The average fiber diameter (AFD) of samples was given as mean \pm standard deviation. FTIR (Fourier transform infrared) spectra of the samples was recorded using the attenuated total reflectance FTIR spectrometer (ATR-FTIR, PerkinElmer, USA) (4000–600 cm^{-1} ; resolution of 4 cm^{-1} ; 64 scans). X-ray diffractometer (Bruker D8 Advance ECO, USA) was the instrument used for the examination crystalline and/or amorphous states of samples (2θ region: 5°–30°; radiation source: Cu-K α ; current/voltage: 25 mA/40 kV). The thermal characteristic of samples was assessed using a thermogravimetric analyzer (TGA, Q500, TA Instruments, USA). Each sample was weighed into a platinum sample pan, and analysis was conducted within the temperature range of room temperature to 550°C in an inert nitrogen environment, with a constant heating rate of 20°C/min. Proton nuclear magnetic resonance ($^1\text{H-NMR}$) spectrometer (Bruker AV500 with autosampler, USA) was utilized to validate the loading of caffeic acid and to approximately quantify the amount of caffeic acid in nanofibrous samples (solvent: d_6 -DMSO; sample concentration: 30 mg/mL; 16 scan). Mestranova software was applied to analyze the $^1\text{H-NMR}$ spectra.

2.6 Disintegration test

The disintegration profiles of CD/caffeic acid and pullulan/caffeic acid nanofibers were evaluated by simulating the artificial saliva³⁴ on the surface of a wet tongue. For this, a filter paper was inserted in disposable Petri dish and then wetted using 10 mL of artificial saliva of which pH was adjusted to 6.8. Then, excess saliva was eliminated from the Petri dish and each sample was positioned centrally on the filter paper. The videos were captured concurrently during the disintegration test (Video S1-5). Time measurement analysis was performed for disintegration test. For this, the time at which the nanofibers interact with medium (t_0) and the moment the solid phase completely dissipates (t_e) were monitored in millisecond and second intervals by high-resolution video recording. The resulting video data were analyzed using the Gemini 3 Flash AI model (Google, USA) to quantify the disintegration kinetics. To minimize timing error, all video recordings at 30 frames per second (fps) were analyzed in detail frame by frame. The pixel intensity difference and edge detection algorithms were employed to analyze the disintegration process. The manual inspection was also performed to verify the reliability of the analysis. The results were reported in the supporting information.

2.7 *In vitro* release test

For time dependent *in vitro* release test, predetermined amount (~ 10 mg) of nanofibrous samples was located into a beaker and subsequently combined with 10 mL of phosphate-buffered saline (PBS) (pH 7.4) solution. The incubator shaker was utilized to agitate the contents of the beakers at 200 rpm (37°C). At designated time intervals (0.5, 1, 2, 4, 6, 8, and 10 min), 0.3 mL was taken from the release system for UV-vis



analysis, and immediately, 0.3 mL of fresh PBS was added to the beaker. UV-vis spectra of the sample solutions taken at various time intervals were obtained throughout the wavelength range of 200–450 nm by a spectrophotometer using a quartz cuvette. The wavelength (216 nm) at which caffeic acid exhibited maximum absorbance was used for calculations and caffeic acid calibration curve ($R^2 \geq 0.99$). The experiments were conducted in triplicate, and the results were presented as release (%) relative to the theoretical amount of caffeic acid incorporated nanofibrous samples. Different kinetic models were applied to examine the release kinetics and the details were given in supporting information.

2.8 Antioxidant activity test

Antioxidant activity of caffeic acid incorporated nanofibrous membrane was evaluated by 2,2-diphenyl-1-picrylhydrazyl (DPPH•) radical scavenging method. The DPPH• radical solution (75 μM) was prepared in methanol. The aqueous solutions of samples at various sample concentrations ranging from 10.4 to 166 $\mu\text{g}/\text{mL}$ were mixed with the DPPH• radical solution to reach a final sample:DPPH volume ratio of 1:6. The mixture was held in dark at the room temperature for 10 min and then absorbance values were recorded at wavelength of 517 nm against methanol by UV-vis spectroscopy. The results, as mean \pm standard deviation, were obtained by triplicate measurements taken for each sample. The DPPH inhibition (%) results were calculated using the following equation;

$$\text{DPPH}\cdot \text{ Inhibition (\%)} = [(A_c - A_s) / A_c] \times 100 \text{ (Eq. 2)}$$

where A_c is the absorbance of the DPPH• radical solution as control, and A_s is the absorbance values of sample solutions. The IC₅₀ values, which denote the minimum amount of sample required to decrease DPPH• absorbance by 50%, were determined using the inhibition values of different nanofiber concentrations.³⁵

2.9 Statistical analyses

Statistical analyses were performed using OriginLab (Origin 2026, USA) to conduct the analysis of variance (ANOVA). Tukey comparison test was applied to ascertain the significant differences across the samples with the 0.05 probability level ($p < 0.05$). All experiments were conducted in triplicate.

2 Results and discussion

3.1 2D-NMR (ROESY) analysis

ROESY NMR spectroscopy was used to examine the spatial arrangement of host–guest interactions in HP β CD/caffeic acid and HP γ CD/caffeic acid ICs. The ROESY spectra showed clear cross-peaks between the inner-cavity protons of HP β CD and HP γ CD (H3 and H5, δ 3.70–4.01 ppm for HP β CD and δ 3.70–4.03 ppm for HP γ CD) and the protons of caffeic acid, indicating close spatial proximity (Fig. 2). In the HP β CD/caffeic acid system, correlations were observed between H3 and H5 and the caffeic acid protons (a, b, c, d, and e), confirming that the guest molecule penetrates the CD cavity (Fig. 2a). Similarly, the HP γ CD/caffeic acid IC exhibited similar interactions between H3

and H5 and the same set of protons (Fig. 2b). These ROESY correlations provide strong evidence that both HP β CD and HP γ CD form ICs by effectively encapsulating the aromatic benzene ring of caffeic acid within their hydrophobic cavities.

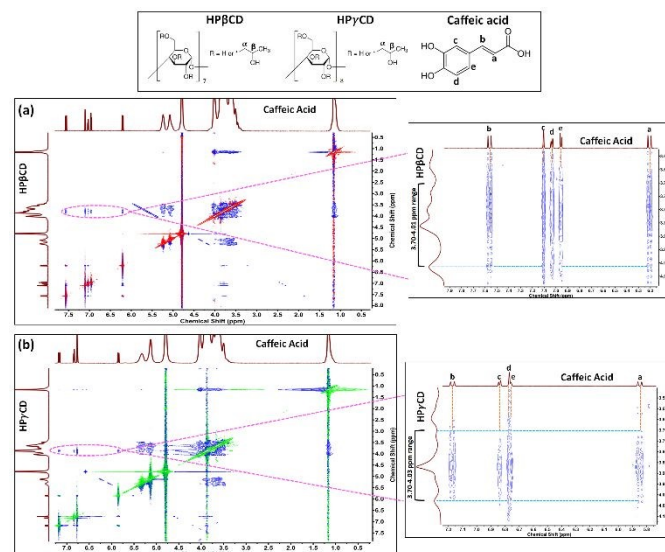


Fig. 2. 2D ROESY spectra of (a) HP β CD/caffeic acid IC, and (b) HP γ CD/caffeic acid IC.

3.2 Phase solubility analysis

To determine the effect of increasing HP β CD and HP γ CD concentrations on the solubility behavior of caffeic acid, phase solubility analysis was performed and phase solubility diagram was plotted as given in Fig. S1. The aqueous solubility of caffeic acid without CD was denoted as $\sim 2.4 \text{ mM}^{13}$, and it was increased by 17.6 and 16.1 times as a result of inclusion complexation with HP β CD and HP γ CD, respectively. The statistical analysis also showed the significant increase in the solubility of caffeic acid due to complex formation ($p < 0.05$) (Fig. S1). On the other hand, the binding constants (K_s) were respectively determined as 37 M^{-1} and 30 M^{-1} for HP β CD and HP γ CD systems using the linear part of the phase solubility diagram, which was obtained under the explained experimental conditions. Even in one of the related studies in which the phase solubility analysis was performed for caffeic acid and HP β CD, numerically identical K_s value was reported as 37 M^{-1} .³⁶ On the other hand, the detected variation between HP β CD/caffeic acid and HP γ CD/caffeic acid systems might be based on the better size match between the caffeic acid and HP β CD cavity, which also provided higher solubility in the case of HP β CD compared to the HP γ CD system ($p < 0.05$) (Fig. S1).³⁷ Additionally, the linear A₁-type phase solubility profiles obtained for both HP β CD/caffeic acid and HP γ CD/caffeic acid systems indicated a predominant 1:1 (CD:guest) complexation stoichiometry between CD and caffeic acid molecules.³⁸

3.3 Morphology analysis

Here, turbid aqueous solutions were obtained for the CD/caffeic acid (1/1) systems, indicating the presence of uncomplexed caffeic acid (Fig. 3a,b-i). On the other hand, CD/caffeic acid



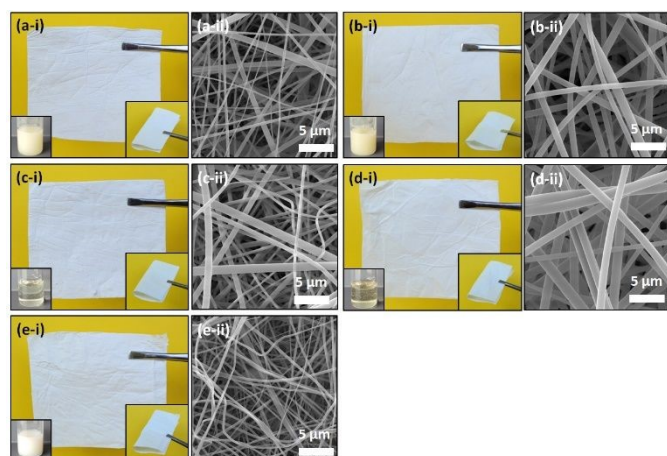


Fig. 3. (i) The photographs of electrospinning solutions and electrospun nanofibers (NF) and (ii) SEM images of (a) HPβCD/Caffeic acid (1/1) NF, (b) HPγCD/Caffeic acid (1/1) NF, (c) HPβCD/Caffeic acid (2/1) NF, (d) HPγCD/Caffeic acid (2/1) NF and (e) Pullulan/Caffeic acid NF.

systems prepared with 2:1 molar ratio (CD:caffeic acid) resulted in clear solutions suggesting the complete complexation between CD and caffeic acid molecules (Fig. 3c,d-i). Pullulan/caffeic acid mixture was also attained with a turbid feature due to the absence of ICs (Fig. 3e-i). Even so, free-standing and readily foldable webs were formed from all given aqueous systems, as shown in Fig. 3a,b,c,d,e-i. Moreover, all these nanofibers were achieved with defect-free and homogenous morphology as demonstrated in the SEM images (Fig. 3a,b,c,d,e-ii). The morphology of electrospun nanofibers can differ due to properties of the electrospinning solution, processing parameters, and the surrounding conditions.

Here, viscosity and conductivity of the solution are critical factors that govern the flow, stretchability, and charge transfer of the electrospinning jet, and so the final morphology of nanofibers.^{17,39} The viscosity and conductivity properties of the electrospinning solutions and the resultant fiber size were represented in Table 1. The average fiber diameter (AFD) values of samples indicated that the high correlation with the viscosity ($r=0.985$) and conductivity ($r=-0.861$) values according to the Pearson correlation coefficients. AFD of HPβCD/caffeic acid (1/1), HPγCD/caffeic acid (1/1), HPβCD/caffeic acid (2/1), HPγCD/caffeic acid (2/1) and pullulan/caffeic acid nanofibers were determined as 435 ± 300 nm, 870 ± 345 nm, 530 ± 205 nm, 1080 ± 285 nm and 270 ± 90 nm, respectively (Table 1). Here, the variation between the viscosity and conductivity values of 1/1 and 2/1 (CD/caffeic acid) systems was not significantly different from each other. Here, HPγCD nanofibers were found to be significantly thicker than HPβCD nanofibers ($p < 0.05$), which is attributed to the higher viscosity and lower conductivity of HPγCD solutions compared to HPβCD ones. This result in a reduced stretching effect on the electrospinning jet, leading to thicker fiber formation (Table 1).^{17,39} On the other hand, pullulan/caffeic acid nanofibers displayed the thinnest fiber formation compared to all other CD/pullulan nanofibers ($p < 0.05$). This was attributed to the high conductivity and low viscosity of pullulan/caffeic acid solution, which led to the high

stretching of the polymer jet, resulting in a reduced fiber diameter (Table 1).

DOI: 10.1039/D6FB00056H

Table 1. The solution properties and the average fiber diameters of resulting electrospun nanofibers.

Sample	Viscosity (Pa-s)	Conductivity ($\mu\text{S}/\text{cm}$)	Average fiber diameter (nm)*
HPβCD/Caffeic acid (1/1)	2.336	28.59	435 ± 300^a
HPγCD/Caffeic acid (1/1)	5.507	6.53	870 ± 345^b
HPβCD/Caffeic acid (2/1)	2.599	30.58	530 ± 205^a
HPγCD/Caffeic acid (2/1)	4.773	6.45	1080 ± 285^c
Pullulan/Caffeic acid	0.711	75.29	270 ± 90^d

*AFD means that do not share a letter are significantly different.

3.4 Structural characterization

FTIR is a common technique to evaluate the formation of IC between CD and guest molecules.⁴⁰ Here, Fig. S2 depicts the FTIR spectra of caffeic acid powder, pristine HPβCD, HPγCD and pullulan nanofibers, and caffeic acid incorporated CD and pullulan nanofibers. HPβCD and HPγCD were identified with the major peaks located at around $3000\text{--}3600$ cm^{-1} , 2930 cm^{-1} , 1650 cm^{-1} , 1370 cm^{-1} and $1020\text{--}1200$ cm^{-1} which respectively corresponds to primary/secondary -OH stretching, C-H stretching, O-H bending, -CH₃ bending and coupled C-C/O and antisymmetric C-O-C stretching vibrations (Fig. S2-a,b).⁴¹ On the other hand, the analogous peaks were also detected for pullulan polymer in the parallel district owing to similar chemical structure with CD molecules (Fig. S2-c).⁴² These are peaks observed at around 3313 cm^{-1} , 2925 cm^{-1} , 1641 cm^{-1} , $1020\text{--}1200$ cm^{-1} and correspond to $\nu(\text{O-H})$ stretching, $\nu(\text{C-H})$ stretching, H-O-H bending, $\nu(\text{C-O})$ stretching, respectively.⁴² For caffeic acid, -OH and -COOH stretching vibration of the benzene ring were observed at around 3403 cm^{-1} and 3218 cm^{-1} (Fig. S2).⁴³ In the case of CD/caffeic acid and pullulan/caffeic acid nanofibers, these peaks were not observed since they were suppressed by the characteristic peaks of CD and pullulan existing in the same region (Fig. S2). The other characteristic peaks of caffeic acid noticed at 1641 cm^{-1} ($\nu(\text{C=O})$), $1617\text{--}1446$ cm^{-1} ($\nu(\text{C=C})$), 1273 cm^{-1} ($\nu(\text{C-OH})$), 1214 cm^{-1} ($\beta(\text{OH}) + \beta(\text{CH})\text{C=C}$), 1118 cm^{-1} ($\beta(\text{CH})$) and 813 cm^{-1} ($\beta(\text{C=O})$) were also observed in the FTIR spectra of CD/caffeic acid nanofibers confirming the presence of caffeic acid in the samples (Fig. S2-a,b).^{43,44} Here, it is worth to mention that these characteristic peaks were seen with inferior intensity in the FTIR spectra of CD/caffeic acid (2/1) nanofibers depending on lower caffeic acid content ($\sim 5\%$ (w/w)) compared to CD/caffeic acid (1/1) nanofibers ($\sim 9\%$ (w/w)) (Fig. S2-a,b). Moreover, apparent shifts (Table S1) were detected for the given caffeic acid peaks in the case of CD/caffeic acid nanofibers demonstrating the IC



formation between caffeic acid and CD molecules (Fig. S2-a,b).⁴⁰ For pullulan/caffeic acid nanofibers, the peak of caffeic acid at 895 cm^{-1} ($\nu(\text{CCO})$) was detected without a shift, and $1617\text{--}1446\text{ cm}^{-1}$ ($\nu(\text{C}=\text{C})$) band just caused an increase in the same region of pullulan/caffeic acid nanofibers (Fig. S2-c). These observations verified the existence of caffeic acid in the absence of interaction within the polymer-based sample.

The crystalline pattern of the samples was examined using the powder XRD (Fig. 4). Caffeic acid having crystalline structure displayed sharp diffraction peaks at 14.1° , 15.8° , 17.5° , 24.4° , 25.7° and 27.0° as seen in its XRD graph (Fig. 4).⁴⁵ For pristine HP β CD, HP γ CD, and pullulan nanofibers, broad XRD peaks were observed due to their amorphous structures. Here, the inclusion complexation between CD and caffeic acid can be followed by disappearance, attenuation or shift of the distinctive peaks of guest caffeic acid.⁴⁰ For all HP β CD/caffeic acid and HP γ CD/caffeic acid nanofibers, similar amorphous pattern of pristine CD was also detected confirming the encapsulation of caffeic acid inside the cavity of CD molecules (Fig. 4a,b). Here, the caffeic acid molecules were separated from each other and could not re-form crystals, and amorphous XRD graphs in the absence of caffeic acid peaks were obtained for CD/caffeic acid nanofibers accordingly. The turbid appearance of CD/caffeic acid (1/1) solutions was attributed to the uncomplexed part of caffeic acid in the systems, as shown in Fig. 3a,b-i. However, this finding did not translate on the XRD results pointing the distribution of the small amount of caffeic acid crystals within the CD/caffeic acid (1/1) nanofibers. On the other hand, the caffeic acid peaks were clearly detected in the

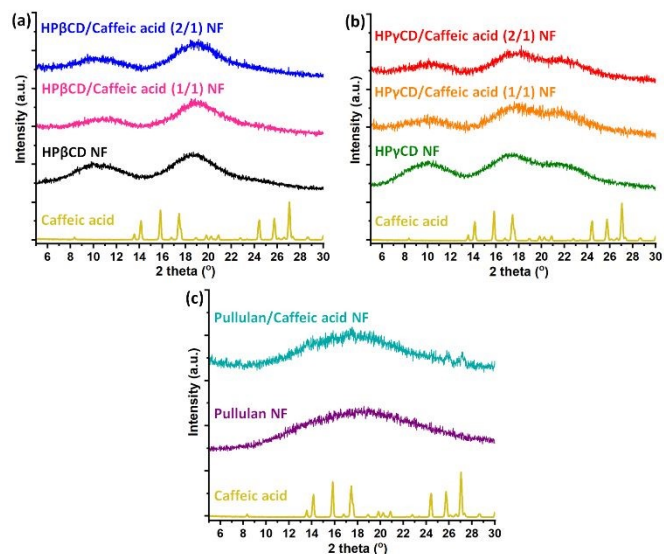


Fig. 4. XRD patterns of Caffeic acid powder, (a) HP β CD NF, HP β CD/Caffeic acid (1/1) NF, HP β CD/Caffeic acid (2/1) NF, (b) HP γ CD NF, HP γ CD/Caffeic acid (1/1) NF, HP γ CD/Caffeic acid (2/1) NF and (c) Pullulan NF, Pullulan/Caffeic acid NF (NF: nanofibers).

XRD graph of pullulan/caffeic acid nanofibers, demonstrating the uncomplexed state of the active compound incorporated in this sample (Fig. 4c).

The thermal degradation profile of samples was characterized by using TGA technique, the thermograms and their derivative (DTG) graphs were presented in Fig. S3. Here, the thermal decomposition of caffeic acid occurred in two stages which is at around 221°C and 300°C , according to DTG curves (Fig. S3). On the other hand, the thermograms of HP β CD and HP γ CD, indicated that the first weight loss below 100°C was due to water loss, whereas the peak decomposition temperatures of substantial weight loss at about 359°C (HP β CD) and 347°C (HP γ CD) were associated with the primary degradations of CDs (Fig. S1-a,b).⁴¹ For CD/caffeic acid (1/1) and CD/caffeic acid (2/1) nanofibers, a three-step weight loss was identified in the thermograms (Fig. S3-a,b). The initial weight loss, happening below 100°C , was the dissipation of water molecules within sample structure. The second weight loss observed at $200\text{--}210^\circ\text{C}$ was associated with the thermal degradation of caffeic acid. The last and the main weight loss step was related to the decomposition of CD ($344^\circ\text{C}\text{--}355^\circ\text{C}$) and overlapped the degradation step of caffeic acid at around 300°C (Fig. S3-a,b). For pristine pullulan nanofibers, two main weight-loss steps were observed: water loss (below 100°C) and degradation of the polymer (328°C) (Fig. S3-c). Pullulan/caffeic acid nanofibers indicated a 3-step thermal degradation profile, like CD/caffeic acid nanofiber, with a small step at 208°C , which corresponded to the decomposition of caffeic acid. Here, it was observed that the first main weight loss step of caffeic acid shifted to lower temperature range ($200^\circ\text{C}\text{--}210^\circ\text{C}$) compared to its pristine state (221°C) in the case of both CD/caffeic acid and pullulan/caffeic acid nanofibers. This might be attributed to the potential interaction of caffeic acid with CD and polymer in a way of encapsulation into the CD cavity and distribution within the polymeric matrix, respectively.²⁷

In this study, $^1\text{H-NMR}$ was utilized for the chemical analysis of samples and to identify the approximate loaded amount of caffeic acid (% w/w) in electrospun nanofibers. Here, the molar ratio of 1:1 and 2:1 (CD:caffeic acid) used for the preparation CD/caffeic acid nanofibers corresponds to $\sim 9\%$ (w/w) and $\sim 5\%$ (w/w) of active agent content for the ultimate samples, respectively. Fig. 5 shows $^1\text{H-NMR}$ spectra of HP β CD/caffeic acid, HP γ CD/caffeic acid and pullulan/caffeic acid nanofibers. The highlighted peaks of each component given in Fig. 5 was used for the calculation of molar ratio and so the caffeic acid content of nanofibers, and it was found that the initial molar ratio values of 1:1 and 2:1 (CD:caffeic acid) was kept for both HP β CD/caffeic acid, HP γ CD/caffeic acid nanofibers. In other words, caffeic acid was preserved over the course of the process, and HP β CD/caffeic acid (1/1), HP γ CD/caffeic acid (1/1) nanofibers, and HP β CD/caffeic acid (2/1), HP γ CD/caffeic acid (2/1) nanofibers were achieved with the initial loading % of ~ 9 and ~ 5 , respectively. Here, it was demonstrated that pullulan/caffeic acid nanofiber was also generated with the initial caffeic acid content of $\sim 5\%$ (w/w). In brief, the quantity of active compound used for the generation of both CD/caffeic acid and pullulan/caffeic acid nanofibers was protected efficiently. It is also worth noting that distinct peaks of caffeic acid were observed for the electrospun nanofibers, in a manner identical to that of the original



compound, suggesting the preservation of its chemical structure (Fig. 5).

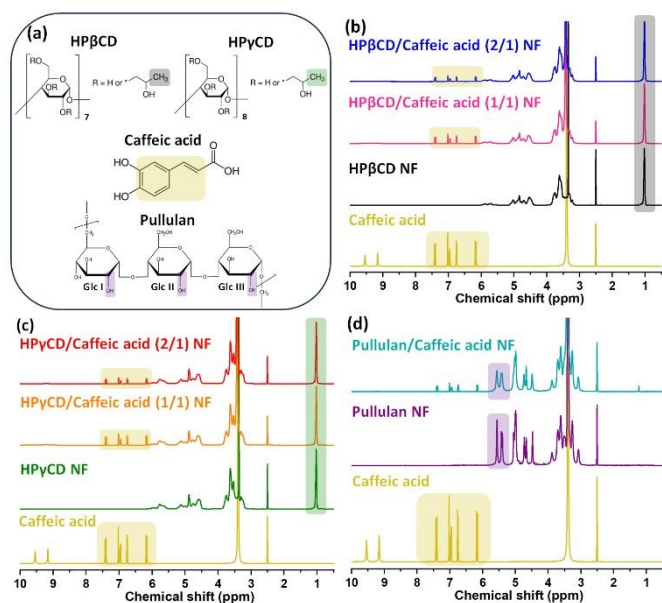


Fig. 5. (a) Chemical structure of HP β CD, HP γ CD and Pullulan. (b) $^1\text{H-NMR}$ spectra of Caffeic acid powder, (a) HP β CD NF, HP β CD/Caffeic acid (1/1) NF, HP β CD/Caffeic acid (2/1) NF, (b) HP γ CD NF, HP γ CD/Caffeic acid (1/1) NF, HP γ CD/Caffeic acid (2/1) NF and (c) Pullulan NF, Pullulan/Caffeic acid NF (NF: nanofibers) (d_6 -DMSO used as solvent).

3.5 Disintegration profiles

The disintegration behavior of CD/caffeic acid and pullulan/caffeic acid nanofibers was examined by simulating the oral cavity medium.³⁴ Fig. 6 indicates the photos captured to represent the disintegration of nanofibers. Additionally, the disintegration times of the samples were monitored with millisecond-level precision, and the obtained results were summarized in Table S2. Here, HP β CD/caffeic acid and HP γ CD/caffeic acid nanofibers were instantly absorbed upon contact with filter paper saturated with artificial saliva and disintegrated in ~ 5 -6 seconds as shown in Fig. 6a,b,c,d. Even though uncomplexed caffeic acid crystals existed in CD/caffeic acid (1/1) nanofibers (Fig. 6a,b), they displayed a similar disintegration profile to CD/caffeic acid (2/1) nanofibers (Fig. 6c,d). On the other hand, pullulan/caffeic acid nanofiber did not behave like CD/caffeic acid nanofibers, though its caffeic acid content is in a crystal state, and could not be immediately absorbed by the wetted filter paper upon contact (Fig. 6e). Additionally, the examined piece of pullulan/caffeic acid nanofibers remained on the petri dish, as a thin transparent layer as shown in Fig. 6e. Here, the superior disintegration of CD/caffeic acid nanofibers compared to pullulan/caffeic acid nanofiber is due to the higher water solubility of hydroxypropylated derivatives of HP β CD and HP γ CD (> 2000 mg/mL) than pullulan polymer (~ 500 mg/mL).⁴⁶ Moreover, the potentially higher content of crystalline caffeic acid in the case of pullulan/caffeic acid nanofiber might have contributed to the lower disintegration performance of the pullulan-based sample.

Nanofibrous feature of samples creates outstanding active sides for the interaction of aqueous medium due to its porous constitution and high surface area by facilitating the penetration of liquid through the structure.⁴⁷ Briefly, CD/caffeic acid nanofibers appear to be more appropriate as an orally fast-disintegrating system, since they would disintegrate in the oral cavity without leaving a grainy mouthfeel, and would ensure an enhanced bioavailability for caffeic acid as a result of its improved water solubility by inclusion complexation.

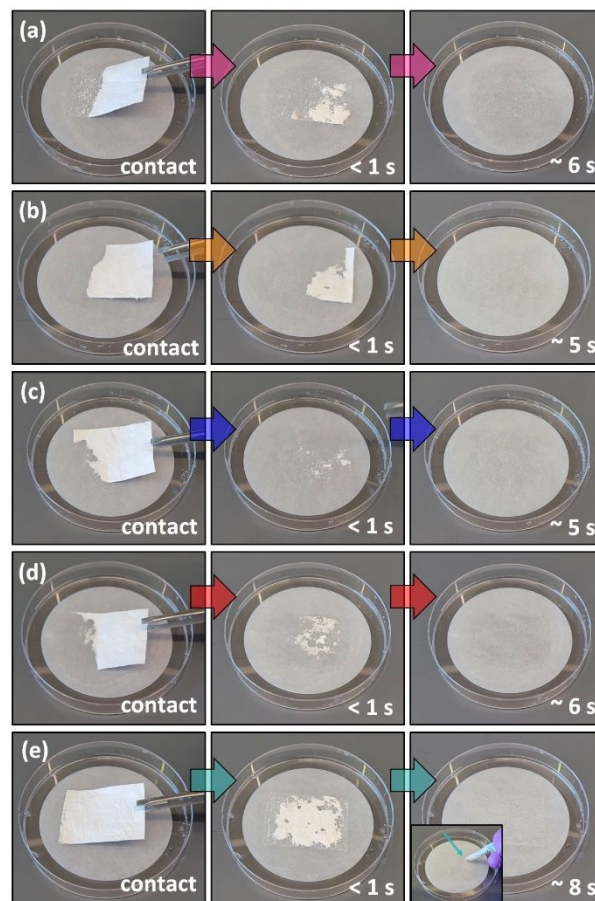


Fig. 6. The disintegration behavior of (a) HP β CD/Caffeic acid (1/1) NF, (b) HP γ CD/Caffeic acid (1/1) NF, (c) HP β CD/Caffeic acid (2/1) NF, (d) HP γ CD/Caffeic acid (2/1) NF and (e) Pullulan/Caffeic acid NF (NF: nanofibers) (The pictures were captured from VideoS1-S5).

3.6 In vitro release profile

The time dependent release of caffeic acid from CD/caffeic acid and pullulan/caffeic acid nanofibers was evaluated in PBS buffer (pH 7.4) and monitored during a 10-minute interval, as shown in Fig. 7. It was found that HP β CD/caffeic acid (1/1), HP γ CD/caffeic acid (1/1), HP β CD/caffeic acid (2/1), HP γ CD/caffeic acid (2/1) nanofibers achieved a release concentration of 89.8 ± 6.8 %, 88.6 ± 6.7 %, 95.5 ± 2.7 % and 91.7 ± 5.5 %, respectively just in 30 seconds. Afterwards, a nearly plateau profile was observed over 10 minutes, reaching the highest release amounts at around 98%, 96%, 100%, and 99%, respectively, for the listed samples mentioned above (Fig. 7a). Here, CD/caffeic acid (2/1) nanofibers indicated slightly higher



maximum release performance compared to CD/caffeic acid (1/1) nanofibers, which are not statistically meaningful ($p > 0.05$) (Table S3), however this might be attributed to the trace amounts of caffeic acid crystals existed in the CD/caffeic acid (1/1) based sample. On the other hand, pullulan/caffeic acid nanofibers only achieved $21.5 \pm 12.6\%$ of release concentration in 30 seconds and reached $78.1 \pm 14.4\%$ at the end of 10-minute interval (Fig. 7a). The performance of pullulan/caffeic acid nanofibers is statistically different and worse than that of CD/caffeic acid nanofibers ($p < 0.05$) (Table S4). In the case of the pullulan-based sample, the release of caffeic acid was highly based on the water solubility of this active compound (~ 2.4 mM). Here, the pullulan matrix formed a barrier for caffeic acid crystals, so its release happened by the exudation into the PBS buffer and then its steady dissolution in this medium. Therefore, a slower and worse release profile was noticed for pullulan/caffeic acid nanofibers compared to CD/caffeic acid nanofibers (Fig. 7a). In other words, the inclusion complexation between CD and caffeic acid and the high aqueous solubility of hydroxypropylated CD types provided an improved solubility and so a superior release performance for caffeic acid compared to a polymeric carrier matrix.

The release of caffeic acid has been also examined using several delivery systems, including liposomes⁴⁸, nanoparticles⁴⁹, nanofibers^{50,51} hydrogel composites⁵², and hydrocolloid-based active films.⁵³ Here, the release of caffeic acid from transferrin-modified liposomes has been reported to be 8% within the initial 4 h and 28% after 8 h under simulated biological conditions (37°C , PBS, pH 7.4).⁴⁸ On the other hand, the caffeic acid-loaded pectin nanoparticles exhibited an initial burst release of approximately $\sim 30\%$ within the first 6 h, followed by a sustained release reaching nearly $\sim 80\text{--}85\%$ over 48 h.⁴⁹ The release study conducted for chitosan nanofibers demonstrated a gradual increase in caffeic acid concentration, reaching $\sim 0.6\text{--}0.7$ mg mL⁻¹ within 30 h, indicating sustained release from the fibrous matrix.⁵⁰ In another related study, gradual increase in caffeic acid concentration was observed for PLA/PCL nanofibrous matrix which reached to $\sim 0.5\text{--}0.8$ mg mL⁻¹ within 24–48 h.⁵¹ In a study on the release pattern of chitosan/collagen composite hydrogels, the release rate depended on the caffeic acid loading amount (5–30% by weight of the polymer solution), with a rapid release observed during the first 60 minutes. Subsequently, the release mechanism stabilized between the first and eighth hours.⁵² Caffeic acid-loaded gelatin/chitosan active films indicated a 30–75% release rate within the first 30 seconds. The time required to reach equilibrium varied with caffeic acid concentration: at lower concentrations (0.5% and 1%), equilibrium was reached within 1–2 hours, whereas at higher concentrations (5% and 10%), equilibrium was established within 3–5 hours.⁵³ Compared with earlier studies on the delivery of caffeic acid, our current work reveals a significant breakthrough in the development of an approach that enables the rapid release of caffeic acid.

In this study, kinetic models were further used to evaluate the release profiles. The R^2 (regression coefficient) values obtained from the calculation of different models were summarized in Table S5. The release behavior of CD/caffeic acid

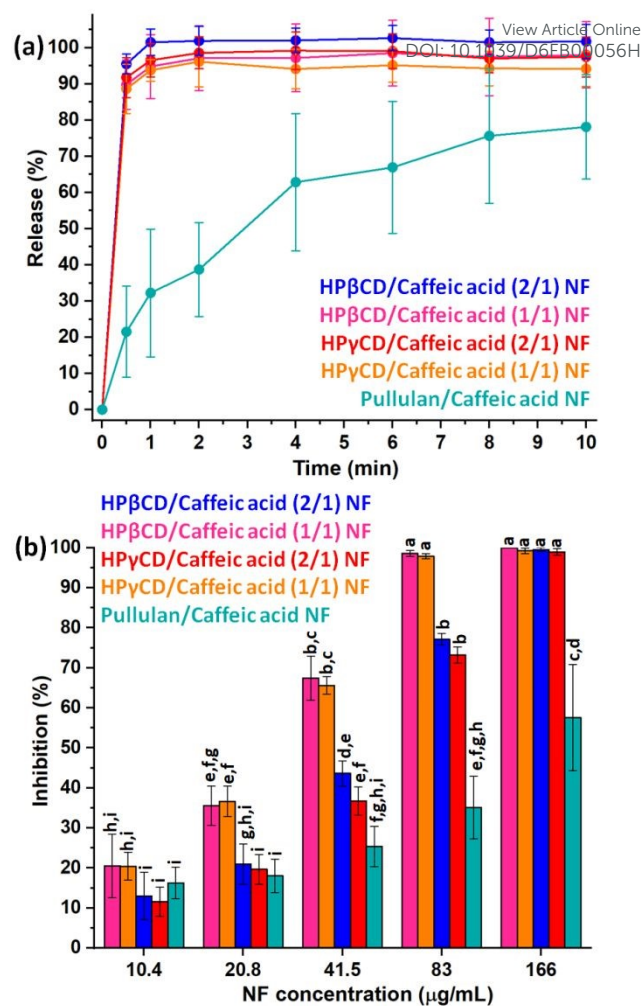


Fig. 7. (a) Time dependent release profiles and (b) antioxidant performance graph of HPβCD/Caffeic acid (1/1) NF, HPγCD/Caffeic acid (1/1) NF, HPβCD/Caffeic acid (2/1) NF, HPγCD/Caffeic acid (2/1) NF and Pullulan/Caffeic acid NF (NF: nanofibers) (Means that do not share a letter are significantly different).

nanofibers did not fit either zero-order or first-order kinetics or the Higuchi model. This revealed that, in the case of CD-based nanofibers, caffeic acid does not release in a time-dependent manner from a planar matrix that is not soluble in water (Fick's first law).⁵⁴ However, the Korsmeyer–Peppas model displayed a relatively better consistency compared to the other kinetic models. In this model, the hydrophilicity and porosity of the carrier system play critical roles, as the initial penetration of water into the pores, followed by its continuous diffusion throughout the matrix, induces significant structural changes such as swelling and/or dissolution of the carrier system. Consequently, the release of the active compounds is predominantly governed by matrix erosion accompanied by subsequent diffusion processes.⁵⁵ Accordingly, the release kinetic analyses confirmed that the release behavior of CD/caffeic acid nanofibers was mainly controlled by erosion and diffusion mechanisms. Moreover, the Korsmeyer–Peppas equations enabled the calculation of the diffusion exponent (n)



values, which were found in the range of $0.45 < n < 0.89$. This finding demonstrated the anomalous (non-Fickian) diffusion behavior, indicating that the release mechanism was driven by the combined effects of caffeic acid diffusion and erosion of the nanofibrous matrix.^{54,56} On the other hand, pullulan/caffeic acid nanofibers showed coherence overall with all applied kinetic models (Table S5), showing the possibility of various manners, including time-dependent, erosion, and diffusion-controlled, during the release of caffeic acid.^{54,56}

3.7 Antioxidant activity profile

Antioxidant compounds can inhibit free radicals and reactive oxygen species (ROS), thus they can eliminate their ruinous outcome, including neurodegenerative diseases, cancer, and stroke, as a consequence of biomolecule (DNA, proteins, lipids) oxidation.⁵⁷ Caffeic acid is a polyphenolic molecule defined by a phenolic ring attached to a hydrocarbon chain which possess an acid group at position 1 and hydroxyl groups at positions 3 and 4 of the ring (Fig. 1). The presence of an additional carbon-carbon double bond adjacent to the benzene ring of this phenolic compound provides strong antioxidant activity by enhancing the conjugated π orbital system.⁴ The antioxidant effect of caffeic acid occurs by the donation of hydrogen from phenol part of this compound to the radical.⁵⁸ In this study, DPPH assay was applied to evaluate the antioxidant potential of CD/caffeic acid and pullulan/caffeic acid nanofibers for the varying concentration of samples (10.4-166 $\mu\text{g}/\text{mL}$). Here, it is worth mentioning that CD and pullulan nanofibers generated in the absence of caffeic acid did not display an antioxidant activity (data are not given). The antioxidant profile of the samples was given as a graph plotted with the radical inhibition (%) values against increasing sample concentration (Fig. 7b). Typically, the scavenging performance of the sample increased with increasing nanofiber concentration (Fig. 7b). For the highest sample concentration (166 $\mu\text{g}/\text{mL}$), HP β CD/caffeic acid (1/1), HP γ CD/caffeic acid (1/1), HP β CD/caffeic acid (2/1), HP γ CD/caffeic acid (2/1) and pullulan/caffeic acid nanofibers showed 100.0 \pm 0.0 %, 99.2 \pm 0.7 %, 99.5 \pm 0.4 %, 98.9 \pm 0.8 % and 57.5 \pm 13.2 % inhibition performance, respectively. For CD/caffeic acid nanofibers, it was found that 1/1-based nanofibers displayed a higher inhibition activity compared to 2/1-based nanofibers due to their higher caffeic acid content (\sim 9 % (w/w)), which is \sim 5 % (w/w) for 2/1 based ones. Even though pullulan/caffeic acid nanofibers were generated having the same caffeic acid content (\sim 5 % (w/w)) as CD/caffeic acid (2/1) nanofibers, they depicted a worse antioxidant performance, especially for high sample concentrations (83 $\mu\text{g}/\text{mL}$ and 166 $\mu\text{g}/\text{mL}$) ($p < 0.05$) (Fig. 7b) (Table S6).

Here, the amorphous state and so the enhanced solubility of caffeic acid, which was obtained as a result of inclusion complexation, is the reason behind the better antioxidant performance of CD/caffeic acid nanofibers compared to pullulan one. In other words, due to the improved physicochemical properties of caffeic acid, a higher amount of active compound was involved in the radical scavenging process in the case of CD/caffeic acid nanofibers. Here, the IC₅₀ value

corresponding to the concentration of the sample, which is necessary to inhibit 50 % of the initial DPPH concentration, was also calculated using the findings of concentration-dependent antioxidant test.³⁵ IC₅₀ values of HP β CD/caffeic acid (1/1), HP γ CD/caffeic acid (1/1), HP β CD/caffeic acid (2/1), HP γ CD/caffeic acid (2/1) and pullulan/caffeic acid nanofibers were determined to be 33.7 $\mu\text{g}/\text{mL}$, 33.9 $\mu\text{g}/\text{mL}$, 52.7 $\mu\text{g}/\text{mL}$, 54.3 $\mu\text{g}/\text{mL}$ and 137.6 $\mu\text{g}/\text{mL}$, respectively. It is also obvious from this finding, a less amount of sample is enough to attain an antioxidant property using CD/caffeic acid (2/1) nanofibers compared to pullulan/caffeic acid one, despite their same caffeic acid content.

Conclusions

In this study, the IC nanofibers of caffeic acid were fabricated using HP β CD and HP γ CD which are highly water-soluble derivatives of modified CDs. Here, IC nanofibers were prepared using the molar ratio of 1:1 and 2:1 (CD:caffeic acid) for both CD types. The nanofibers of IC-free pullulan/caffeic acid were also produced for the comparative examinations. All free-standing nanofibers were attained with homogenous morphology. The penetration of caffeic acid into HP β CD and HP γ CD cavities by inclusion complexation was confirmed with the 2D-NMR measurement. Phase solubility findings showed that the aqueous solubility of caffeic acid can be increased by \sim 18- and 16-fold using HP β CD and HP γ CD, respectively, through inclusion complexation, while XRD results indicated the amorphization of caffeic acid crystals. The complexation between caffeic acid and CD molecules was also demonstrated by FTIR technique. ¹H-NMR findings revealed the preservation of both the chemical structure and the initial contents (\sim 9 % and \sim 5 % (w/w)) of caffeic acid within the nanofibrous samples of CD/caffeic acid (1/1), CD/caffeic acid (2/1), and pullulan/caffeic acid. CD/caffeic acid nanofibers disintegrated in an artificial saliva environment in \sim 5-6 seconds, while a thin transparent layer remained from pullulan/caffeic acid nanofibers. Additionally, CD/caffeic acid nanofibers displayed superior release profile in aqueous environment compared to pullulan/caffeic acid nanofibers by releasing \sim 90-95 % of caffeic acid just in 30 seconds. Furthermore, better antioxidant activity was obtained in the case of CD/caffeic acid nanofibers. Here, the enhanced solubility of caffeic acid through inclusion complexation, the higher water solubility of HP β CD and HP γ CD ($>$ 2000 mg/mL) compared to pullulan (\sim 500 mg/mL), and the highly porous structure of the electrospun nanofibers are key factors in yielding the fast-release, fast-disintegration, and enhanced antioxidant features. To conclude, the exclusive properties of both the electrospun nanofibrous web and the CDs were combined to generate an alternative formulation for the oral administration of caffeic acid as a fast-disintegrating delivery system. Here, polymer-free CD/caffeic acid nanofibrous webs were produced using completely biocompatible sources of CD, caffeic acid, and water in the absence of an additional toxic chemical or solvent. This sustainable approach can be especially attractive for biomedical, food, and cosmetic-based applications and can be a promising step for the development



of biomaterials by eliminating the environmental and health loadings originating from the use of fossil fuel-based products.

Author contributions

A. C.: Data curation, Formal analysis, Conceptualization, Methodology, Validation, Investigation, and Writing - original draft. K. E.: Investigation, Writing – original draft. M. A.: 2D-NMR investigation and writing. T. U.: Supervision, Resources, Conceptualization, Methodology, Project administration, Funding acquisition, Review & Editing.

Conflicts of interest

The authors declare that they have no known competing financial interests or personal ties that could appear to have influenced the work revealed in this paper.

Data availability

The data supporting this article have been included as part of the Supplementary Information (SI). Supplementary information: Table S1 cited in Section 3.4, Tables S2 cited in Section 3.5, Tables S3-5 cited in Section 3.6, Tables S6 cited in Section 3.7, Fig. S1 is cited in the Section 3.2, Fig. S2 is cited in the Section 3.4, Fig. S3 is cited in the Section 3.4. Video S1-S5 show fast-disintegration profiles of samples. See DOI: <https://doi.org/XXX>

AI use statement

During the preparation of this manuscript, the authors utilized the Gemini 3 Flash (Google) artificial intelligence model to perform objective analysis of video-based disintegration experiments. The AI-assisted workflow was employed for temporal image processing and quantification of morphological changes in nanofibers throughout the disintegration process. All AI-generated outputs, including time-resolved data and analytical observations, were subsequently reviewed and verified by the authors to ensure scientific accuracy and reliability. The authors assume full responsibility for the integrity of the data, analyses, and interpretations presented in this study.

Acknowledgements

This work made use of the Cornell Center for Materials Research Shared Facilities, and the Cornell Chemistry NMR Facility supported in part by the NSF MRI program (CHE-1531632), and the Fiber Science & Apparel Design facilities. K.E. thanks The Scientific and Technological Research Council of Turkey (TUBITAK) for the financial support (TUBITAK-BIDEB 2214A Fellowship program).

References

- 1 N. Kumar and N. Goel, *Biotechnol. Reports*, 2019, e00370.
- 2 S. Al Jitan, S. A. Alkhoodri and L. F. Yousef, *Phenolic Acids From Plants : Extraction and Application to Human Health*, Elsevier B.V., 1st edn., 2018, vol. 58.
- 3 D. Liu, S. Pan and J. Sun, *Int. J. Food Microbiol.*, 2025, 111413.
- 4 A. Purushothaman, S. S. Babu, S. Naroth and D. Janardanan, *Free Radic. Res.*, 2022, **56**, 617–630.
- 5 M. Yazar, M. Sevindik, I. Uysal and A. O. Polat, , DOI:10.1007/s11094-025-03363-7.
- 6 A. Kowalczyk, C. Ignazio and G. Tuberoso, 2025, **2**, 1–16.
- 7 S. Mirzaei, M. Hossein, A. Zabolian and H. Saleki, *Pharmacol. Res.*, 2021, **171**, 105759.
- 8 F. Paulo and L. Santos, *Dry. Technol.*, 2019, **37**, 950–961.
- 9 N. P. Katuwavila, A. D. L. C. Perera, V. Karunaratne, G. A. J. Amaratunga and D. N. Karunaratne, *J. Nanomater.*, 2016, 9701870.
- 10 L. Lin, S. Peng, X. Chen, C. Li and H. Cui, *Int. J. Biol. Macromol.*, 2023, **241**, 124591.
- 11 G. S. Guler, G. Sumnu and N. Yazicioglu, *Food Bioprocess Technol.*, 2024, **17**, 5338–5356.
- 12 R. Shiozawa, Y. Inoue, I. Murata and I. Kanamoto, *asian J. Pharm. Sci.*, 2018, **13**, 24–33.
- 13 M. Kfoury, C. Geagea, S. Ruellan, H. Greige-Gerges and S. Fourmentin, *Food Chem.*, 2019, **278**, 163–169.
- 14 Sema Zeren, S. Sahin and G. Sumnu, *Foods*, 2022, **11**, 1860.
- 15 M. G. Ignatova, N. E. Manolova, I. B. Rashkov, N. D. Markova, R. A. Toshkova, A. K. Georgieva and E. B. Nikolova, *Mater. Sci. Eng. C*, 2016, **65**, 379–392.
- 16 G. Oh, S. Ko, J. Je, Y. Kim and J. Oh, *Int. J. Biol. Macromol.*, 2016, **93**, 1549–1558.
- 17 G. F. Elfawal, A. O. Šišková and A. E. Andicsová, *Fibers Polym.*, 2025, **26**, 4133–4160.
- 18 C. Wang, Y. Su and J. Xie, *Accounts Mater. Res.*, 2024, **5**, 987–999.
- 19 F.-L. Sun, M.-Y. Zhao, Y. Li, Z.-Y. Li, X.-J. Li, N. Wang, B.-W. Hu, H.-Y. Xue, M. Zhao and J.-L. Tian, *Food Hydrocoll.*, 2025, **158**, 110474.
- 20 S. Hussain, R. Akhter and S. S. Makeddar, *Sustain. Food Technol.*, 2024, **2**, 1297–1364.
- 21 A. Matencio, S. Navarro-Orcajada, F. García-Carmona and J. M. López-Nicolás, *Trends food Sci. Technol.*, 2020, **104**, 132–143.
- 22 P. Singh and R. Mahar, *Int. J. Pharm.*, 2024, **662**, 124485.
- 23 Y. Inoue, K. Suzuki, T. Ezawa and I. Murata, *J. Incl. Phenom. Macrocycl. Chem.*, 2015, **83**, 289–298.
- 24 B. Balusamy, A. Celebioglu, A. Senthamizhan and T. Uyar, *J. Control. release*, 2020, **326**, 482–509.
- 25 A. Celebioglu and T. Uyar, *Food Chem.*, 2020, **317**, 126397.
- 26 Z. I. Yildiz, F. Topuz, M. E. Kilic, E. Durgun and T. Uyar, *Food Chem.*, 2023, **423**, 136284.
- 27 A. Celebioglu, D. Tekant, M. E. Kilic, E. Durgun and T. Uyar, *ACS Food Sci. Technol.*, 2022, **2**, 568–580.
- 28 A. Celebioglu and T. Uyar, *Int. J. Pharm.*, 2020, **584**, 119395.
- 29 F. Topuz and T. Uyar, *Expert Opin. Drug Deliv.*, 2025, **22**, 957–969.



- 30 F. Laffleur and V. Keckeis, *Int. J. Pharm.*, 2020, **590**, 119912. 57 I. Gülçin, *Arch. Toxicol.*, 2012, **86**, 345–391. [View Article Online](#)
- 31 D. PR and P. Sudheer, *Ind. Appl. Funct. Foods, Ingredients Nutraceuticals*, 2023, 361–396. 58 F. A. Khan, A. Maalik and G. Murtaza, *J. Food Drug Anal.*, 2016, **24**, 695–702. DOI: 10.1016/j.jfda.2015.05.005
- 32 V. Narayanan, M. Alam, N. Ahmad, S. B. Balakrishnan, V. Ganesan, E. Shanmugasundaram, B. Rajagopal and S. Thambusamy, *Spectrochim. Acta - Part A Mol. Biomol. Spectrosc.*, 2021, **249**, 119308.
- 33 K. R. Sugumaran and V. Ponnusami, *Carbohydr. Polym.*, 2017, **173**, 573–591.
- 34 Y. Bi, H. Sunada, Y. Yonezawa, K. Danjo, A. Otsuka and K. IIDA, *Chem. Pharm. Bull.*, 1996, **44**, 2121–2127.
- 35 İ. Gulcin, *Arch. Toxicol.*, 2025, 1–105.
- 36 E. Pinho, G. Soares and M. Henriques, *J. Microencapsul.*, 2015, **32**, 804–810.
- 37 L. Szente and É. Fenyvesi, *Struct. Chem.*, 2017, **28**, 479–492.
- 38 T. Loftsson, D. Hreinsdóttir and M. Másson, *Int. J. Pharm.*, 2005, **302**, 18–28.
- 39 B. O. Omiyale, A. Ogbeyemi, A. A. Rasheed, T. M. Adamolekun and W. C. Zhang, *Next Nanotechnol.*, 2025, **8**, 100295.
- 40 P. Mura, *J. Pharm. Biomed. Anal.*, 2015, **113**, 226–238.
- 41 C. Yuan, B. Liu and H. Liu, *Carbohydr. Polym.*, 2015, **118**, 36–40.
- 42 P. Shao, B. Niu, H. Chen and P. Sun, *Int. J. Biol. Macromol.*, 2018, **107**, 1908–1914.
- 43 M. Shen, J. Zhou, M. Elhadidy, Y. Xianyu, J. Feng, D. Liu and T. Ding, *Ultrason. Sonochem.*, 2022, **86**, 106003.
- 44 R. Świsłocka, *Spectrochim. Acta Part A Mol. Biomol. Spectrosc.*, 2013, **100**, 21–30.
- 45 J. Liu, X. Wang, R. Bai, N. Zhang, J. Kan and C. Jin, *Starch-Stärke*, 2018, **70**, 1700141.
- 46 T. Loftsson and M. E. Brewster, *J. Pharm. Pharmacol.*, 2010, **62**, 1607–1621.
- 47 D.-G. Yu, J.-J. Li, G. R. Williams and M. Zhao, *J. Control. release*, 2018, **292**, 91–110.
- 48 S. Andrade, M. C. Pereira and J. A. Loureiro, *Colloids Surf. B: Biointerfaces*, 2023, **225**, 113270.
- 49 S. Zhou, Z. Yu, W. Yao, M. Wang, Y. Yang, J. Qin, X. Wu and C. Guo, *Colloids Surf. B: Biointerfaces*, 2025, **247**, 114419.
- 50 P.-H. Chiu, Z.-Y. Wu, C.-C. Hsu, Y.-C. Chang, C.-M. Huang, C.-T. Hu, C.-M. Lin, S. C. Chang, H.-J. Hsieh and C.-A. Dai, *Rsc Adv.*, 2024, **14**, 34756–34768.
- 51 M. B. Reyhanoglu, R. B. Sulutas, B. Adali, E. Kaya, G. B. Tinaz, S. Evran, O. Gunduz and S. Cesur, *Eur. J. Pharm. Biopharm.*, 2026, 115054.
- 52 K. Thongchai, P. Chuysinuan, T. Thanyacharoen, S. Techasakul and S. Ummartyotin, *J. Mater. Res. Technol.*, 2020, **9**, 6512–6520.
- 53 N. Benbettaieb, J. Nyagaya, A.-M. Seuvre and F. Debeaufort, *J. Agric. Food Chem.*, 2018, **66**, 6906–6916.
- 54 N. A. Peppas and B. Narasimhan, *J. Control. release*, 2014, **190**, 75–81.
- 55 R. W. Kormeyer, R. Gurny, E. Doelker, P. Buri and N. A. Peppas, *Int. J. Pharm.*, 1983, **15**, 25–35.
- 56 X. Li, M. A. Kanjwal, L. Lin and I. S. Chronakis, *Colloids Surf. B: Biointerfaces*, 2013, **103**, 182–188.



Data availability

The data supporting this article have been included as part of the Supplementary Information (SI). Supplementary information: Table S1 cited in Section 3.4, Tables S2 cited in Section 3.5, Tables S3-5 cited in Section 3.6, Tables S6 cited in Section 3.7, Fig. S1 is cited in the Section 3.2, Fig. S2 is cited in the Section 3.4, Fig. S3 is cited in the Section 3.4. Video S1-S5 show fast-disintegration profiles of samples. See DOI: <https://doi.org/XXX>

